석사학위논문

Interannual modulation of Kuroshio intensity in the East China Sea Over the Past Three Decades

제주대학교 대학원

지구해양융합학부
지구해양전공

조 성 현

2023년 2월

Interannual modulation of Kuroshio intensity in the East China Sea Over the Past Three Decades

지도교수 문 재 홍

조 성 현

이 논문을 이학 석사학위 논문으로 신청함

2022 년 12 월

조성현의 이학 석사학위 논문을 인준함

심사위원장   문 재 홍   ㊞

위   원   송 상 근   ㊞

위   원   김 태 균   ㊞

제주대학교 대학원

2022 년 12 월

Interannual modulation of Kuroshio intensity in the East China Sea Over the Past Three Decades

Seonghyun Jo

(Supervised by Professor Jae-Hong Moon)

A thesis submitted in partial fulfillment of the requirement for the degree of Master of Science

December 2022

This thesis has been examined and approved.

....

Thesis director, Jae-Hong Moon, Prof. of Earth Marine Sciences

....

Sang-Keun Song, Prof. of Earth Marine Sciences

....

TaeKyun Kim, Dr. of Earth Marine Sciences

Date 2022. 12.

Faculty of Earth and Marine Convergence

GRADUATE SCHOOL

JEJU NATIONAL UNIVERSITY

Index

List of Figure

Abstract

Previous studies have suggested that westward-migrating mesoscale eddies are a dominant factor that modulate the interannual Kuroshio intensity in the East China Sea (ECS), indicating a close positive correlation between them. According to the extended record of altimetry-based sea level anomalies (SLAs) until 2020, however, the interannual variation of the Kuroshio intensity no longer has a strong positive correlation with eddy activity in the subtropical countercurrent (STCC) region since the early 2000s. Our observational analyses showed that the Kuroshio intensity in the ECS can be modulated by the combined effect of westward-migrating mesoscale eddies and westward-propagating oceanic planetary waves from the east. Until the early 2000s, the interannual variability of Kuroshio was mainly affected by eddy migration from the STCC region, associated with oceanic instability driven by large-scale wind patterns over the western North Pacific. Since then, oceanic planetary waves propagating westward across the Pacific basin have largely modulated the interannual variability of the ECS-Kuroshio intensity by superimposing the SLAs related to mesoscale eddies that propagated towards the east of Taiwan.

1. Introduction

Originating from the North Equatorial current (NEC), the Kuroshio current entering the East China Sea (ECS), passes through the east of Taiwan to the south of Japan, transports heat northward from the tropics, and modulates the regional ocean and climate along its path (Gan *et al.*, 2019; Yang *et al.*, 2018). The Kuroshio current has an average of 18~22.5 Sv in the East China Sea, having a wide spectrum from semi-seasonal to decadal. In addition to substantial seasonal variability, the Kuroshio current exhibits strong variability, especially by interacting with mesoscale oceanic waves at the East Taiwan channel (ETC). Due to the topographic location, ETC serves as an arrival point of the westward propagating waves generated along the band of 18~25N (**Figure 1**). The alteration of the atmospheric condition contributes to the generation of westward propagating Rossby waves and mesoscale eddy activities by disturbance to the oceanic state. To the east of Taiwan, a weak surface eastward current flows against the westerlies, accompanied by the subsurface temperature and density front placed on the edge of NEC's northern branch. The subsurface front forms the baroclinically unstable structure yielding westward migrating mesoscale eddies that collide frequently with the Kuroshio Current east of Taiwan. The eddies generally adjust the 3~5Sv of Kuroshio's transport volume (Chang et al 2018), giving a dominant effect in high frequency to decadal variability of the Kuroshio intensity. Though active research was conducted to understand the high-frequency variability (i.e., several days to seasonal) of Kuroshio intensity related to mesoscale eddies arriving in the area east of Taiwan (Yang *et al.*, 1999; Qiu *et al.*, 1999; Johns *et al.*, 2001), however, the Kuroshio variability on interannual and longer timescales is currently poorly understood because of the limited in situ measurements available at longer time scales.

Recent advances in satellite altimetry have enabled the estimation of the interannual

제주대학교 중앙도서관
JEJU NATIONAL UNIVERSITY LIBRARY

Kuroshio variability in the ECS. Andres et al. (2011) showed a strong correlation between the Kuroshio intensity and the Pacific Decadal Oscillation (PDO) index on interannual to decadal timescales using altimetry records from 1993 to 2008. They argued that there were two different mechanisms that PDO-like WSC pattern over the western north pacific modulates the Kuroshio intensity. One is an instant effect of the fast barotropic waves induced by the wind pattern that has several months of time lags with KVT. The other is the slow baroclinic waves generated on the eastern side of the north pacific, traveling parallelly to the latitude with seven years of time lags. Meanwhile, recent studies suggest that westward propagating mesoscale eddies from the Subtropical Countercurrent region play a crucial role in modulating the interannual variability of the Kuroshio Current in the ECS rather than linear oceanic waves (Hsin *et al* 2011; Yan *et al* 2016). Chang and Oey 2011 focused on the role of eddy activity in the STCC near the east of Taiwan. They found a strong correlation between the interannual Kuroshio intensity and EKE in the STCC based on altimetry sea surface height (SSH) and 29 years of tide-gauge data. They argued that the interannual variability of the Kuroshio transport is directly affected by its interaction with westward-propagating eddies from the STCC within 20–23°N.

In interannual to the decadal time scale, the WSC pattern over the western north pacific is a crucial factor in the relationship between eddy activities and Kuroshio intensity. Chang and Oey 2013 reported interannually variating dipole WSC patterns over the western north pacific control baroclinic instability of the North Equatorial Current (NEC)-STCC system. The WSC pattern modulates the meridional Ekman transport and gradient of the subsurface front, leading to the interannual fluctuation of the EKE. The dipole WSC pattern was also presented by Qiu and Chen (2010, 2013), suggesting PDO-related wind forcing and surface heat flux forcing modulate the EKE in STCC. Hsin *et al.* (2013) also reported that the interannual variability of the Kuroshio east of Taiwan is modulated by westward-propagating eddies induced by large-

scale wind forcing in the western North Pacific, emphasizing the contribution of the relative intensity of anticyclonic versus cyclonic eddies east of Taiwan. Although there is still debate about the cause of the variability of the Kuroshio intensity, most studies mentioned above agree on the impact of PDO-related eddy activities in the STCC region on the interannual modulation of the Kuroshio in the ECS.

On the other hand, recent analyses of observations and ocean models have revealed that the high coherence between the Kuroshio intensity and PDO index has deteriorated since the late 1990s and/or the early 2000s (Nakamura *et al.,* 2012; Soeyanto *et al.,* 2014; Wu *et al.,* 2019). Soeyanto *et al.,* (2014) found that the well-known correlation between the two has disappeared since roughly 2002. A more recent analysis by Wu *et al.* (2019) supported this disassociation of the ECS-Kuroshio with the PDO, yielding an insignificant correlation of 0.03 for the period 1993–2013. They discussed that the disassociation might be related to changes in atmospheric circulation during a warming "hiatus" in the 2000s, which is closely linked to the phase shift of PDO (England *et al.,* 2014; Maher *et al.,* 2018).

The Kuroshio Current plays an important role in weather and climate through heat transport and air-sea interaction processes. Therefore, it is essential to understand how and why the Kuroshio intensity has changed over the past decades. Despite the importance of the climate system, the following aspects remain unclear: (i) the dominant mode that represents changes in the Kuroshio intensity in the ECS, (ii) how Kuroshio transport has varied interannually over the past three decades, and (iii) the key factors that modulate the interannual variability of Kuroshio intensity in the ECS. Herein, these issues are revisited by analyzing an extended record of satellite altimetry datasets until 2020 and several climate datasets. This master's thesis is based on the publication in Frontiers in marine science, "Interannual modulation of the Kuroshio in the East China Sea over the Past Three decades" (Jo et al 2022).
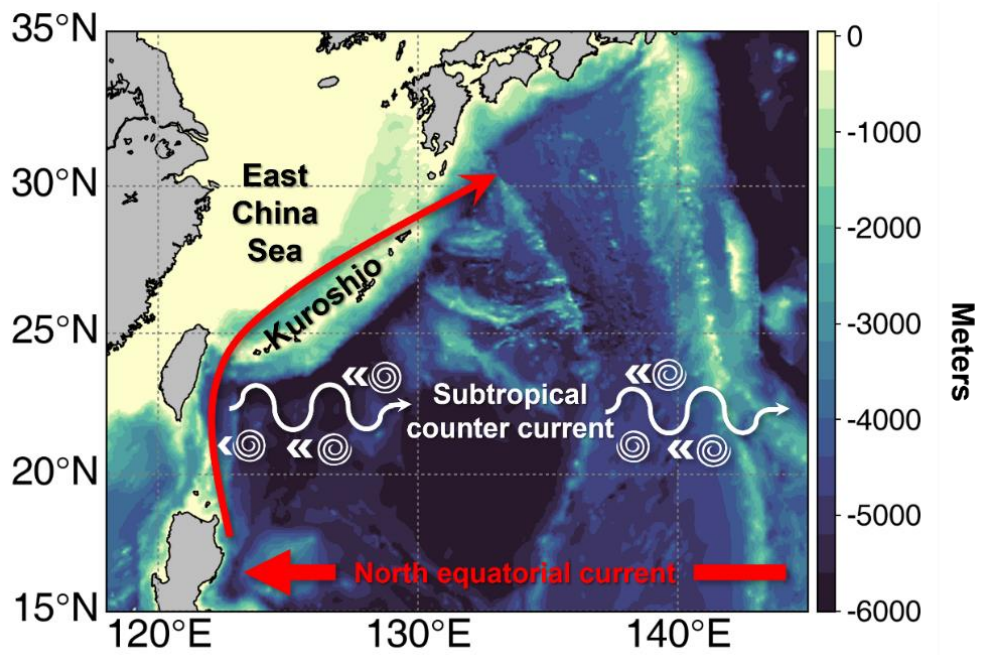
Figure 1. Schematic depiction of main currents and topography of the western north pacific.

2. Data and method

2.1 Satellite altimetry

Satellite altimetry products from 1993 to 2020 were used in this study. The dataset comprises daily sea level anomaly (SLA) and geostrophic velocity with a resolution of 1/4°×1/4° obtained from the Copernicus Climate Change Service (C3S; https://cds.climate.copernicus.eu/). This dataset is produced to the analysis the ocean and climate indicators by merging two-satellite constellations at all time steps. The monthly averaged data fields were computed from daily altimetry data over the 28-year period, and the global sea level trend was eliminated grid-by-grid to remove the thermostatic effect.

For the identification of the mesoscale eddy activities, eddy kinetic energy (EKE) was calculated from gridded altimetry data based on geostrophic balance.

$$\text{EKE} = \frac{1}{2}(u' + v') \qquad (1)$$

where u' and v' indicate the surface geostrophic current anomalies, $u' = \frac{g}{f}\frac{\partial h'}{\partial y}, v' = -\frac{g}{f}\frac{\partial h'}{\partial x}$, h' denotes the SLA, f is the Coriolis parameter, and g is the gravitational acceleration.

2.2 Wind data

Two wind dataset was utilized for the comparison and verification. One is surface wind data of the ERA5 reanalysis product from the European Center for Medium-Range Weather Forecasts (ECMWF). The ERA5 dataset covers the period from Jan 1959 to near real-time, produced by the 4D-Var data assimilation method with 137 hybrid sigma/pressure levels and model forecasts of the ECMWF Integrated Forecast System (IFS). The other is NCEP/NCAR

5

reanalysis-1 data from *the National Centers for Environmental Prediction* (https://psl.noaa.gov/data/gridded/data.ncep.reanalysis.html). Monthly gridded data with a resolution of 1/4° are available at C3S. The NCEP/NCAR Reanalysis data set is a continually updated (1948–present) globally gridded dataset incorporating observations and outputs of the numerical weather prediction (NWP) model from 1948 to the present.

The wind stress curl was calculated by cross product of the del operator and wind stress i.e.,

$$\nabla \times \tau$$

And the magnitude of the surface wind stress τ is calculated as a function of wind speed with the following equation:

$$\tau = \rho C_D U^2$$

Where ρ is the density of the surface layer assumed as constant value 1018hpa, C_D is wind drag coefficient 0.0015.

2.3 Oceanic and climate indices

PDO index was also used to represent the climate variability over the western North Pacific. The monthly time series of the PDO index was obtained from the National Centers for Environmental Information of NOAA (https://www.ncdc.noaa.gov/teleconnections/pdo/). PDO is defined by the leading pattern of sea surface temperature anomalies in the North Pacific basin. Positive values of the PDO index correspond with negative SST anomalies in the central and western North Pacific and positive anomalies in the eastern North Pacific. Oscillation of the SST and corresponding atmospheric conditions contributes to upper ocean baroclinic stability and generation of linear Rossby waves.

To quantify the EKE variability of the STCC, we obtained time series of the leading pattern of the EKE in STCC by applying EOF to the EKE data. This method was previously used by Qiu and Chen 2013 to investigate the mechanism of interannual to the decadal fluctuation of

6

EKE in STCC. The leading mode and pc time series are shown in **Figure 2** with a direct calculation of spatial mean EKE over the STCC.

We estimated the proxy of Kuroshio intensity east of Taiwan by adopting and computing the empirical Kuroshio volume transport (KVT) index proposed by Yan and Sun 2015. This index is computed based on the linear relationship between observation and sea level difference (SLD) from altimetry SLAs. They suggested that this altimetry-based index serves as a good proxy for volume transport of the Kuroshio east of Taiwan.

$$KVT = 0.31 \times SLD + 6.55 \ (Sv) \qquad (2)$$

The SLD between two locations P1 and P2 (123.5°E, 24°N and 123.25°E, 27.25°N), was used as an optimal estimator for the KVT to the east of Taiwan.

(a)

(b)

(c)
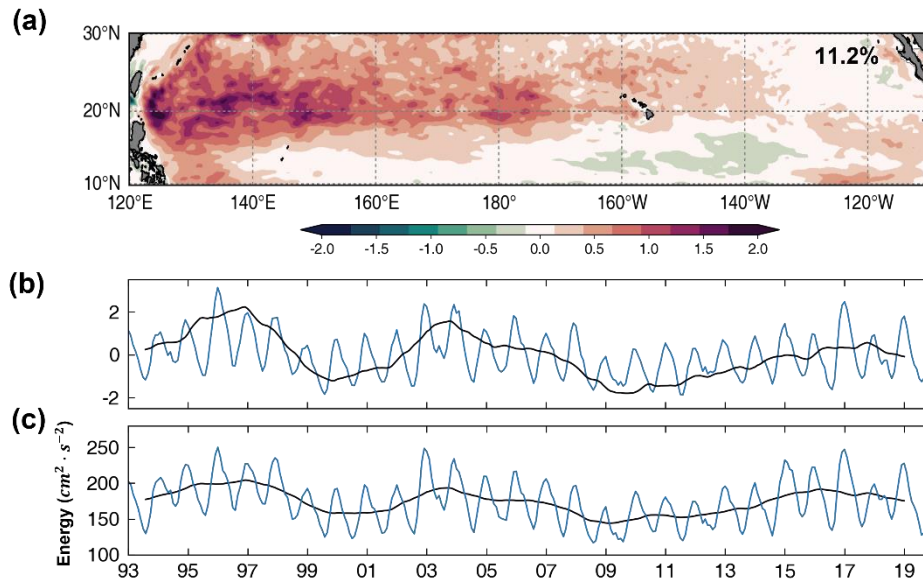
Figure 2.   Spatial pattern of the first-leading mode of EKE in STCC depicted from AVSIO during 1993-2020. Corresponding pc time series (blue) and their two years running average (thick blue line). Time series of a spatial average of EKE and its two years running average (thick blue line).

8

2.4 EOF analysis

The EOF analysis is widely used in various study areas to identify spatial patterns of variability and their change with time. It transforms the dataset into mathematically orthogonal modes, which could be interpreted as oceanic/atmospheric structures. The method computes a spatially weighted covariance anomaly matrix from the dataset and finds its eigenvalues and eigenvectors. The eigenvalues provide information on the percentage of variances explained by each mode. The PC time series of each mode are determined by projecting the eigenvectors onto spatially weighted anomalies, which explains the variability of each mode over time. As in the case of Qiu and Chen 2013, EOF was used in this study to identify the most dominating structure of dataset in the research area. The mathematical expression of the EOF analysis is as follows (Hannachi et al. 2007).

Suppose that $X(t, s)$ represents the value of time-space filed X. Then, X can be represented by the matrix,

$$X = (x_1, x_1, \ldots, x_n)^T = \begin{pmatrix} x_{11} & \cdots & x_{1p} \\ \vdots & \ddots & \vdots \\ x_{n1} & \cdots & x_{np} \end{pmatrix}$$

Where, $x_t = (x_{t1}, x_{t1}, \ldots, x_{tp})^T$, and $t = 1, \ldots, n$, represents the value of the field at time. The climatological average of data field can be denoted as

$$\bar{x} = (\bar{x}_1, \ldots \ldots, \bar{x}_p) = \frac{1}{n} 1_n^T X$$

where, 1_n is the column vector having length of n, and $\bar{x}_i$ is time average of i'th spatial grid points which is $\bar{x}_i = \frac{1}{n} \sum_{k=1}^n x_{k,i}$. Thus, anomaly of data field is:

$$X' = X - 1_n \bar{x}$$

Once the anomaly of matrix of data defined, then, covariance matrix is defined by:

$$S = \frac{1}{n} X'^T X'$$

9

Which element of S, $s_{i,j}$ is covariance between the time series of any grid point (s_i, s_j). The empirical orthogonal functions (EOFs) are obtained as the solution to the eigenvalue problem:

$$Su = \lambda^2 u$$

The k'th eigen vector of the S, u_k is to be the k'th EOF. The eigenvalue λ_k explains the variance that k'th EOF accounted for in percentage as:

$$\frac{100\lambda_k^2}{\sum_{k=1}^{p} \lambda_k^2} \%$$

The k'th PC time series is the projection of the anomaly field X onto the k'th EOF, whose elements a_{ik}, $t = 1, \dots n$ are given by:

$$a_{ik} = \sum_{j=1}^{p} x_{i,j} u_{k,j}$$

2.5 Numerical model

The Regional Ocean Modeling System (ROMS) uses a primitive equation with static equilibrium and Bushnesque approximation applied to the Navia-Stokes equation. The horizontal grid of ROMS is an Arakawa-C grid, where the UV components are calculated at the edges of each grid, while scalar variables are calculated at the center. This stagged structure enhances the stability of volume conservation (Arakawa and Lamb, 1997). For the vertical coordinates, ROMS has a terrain-following coordinates system. The terrain-following vertical coordinate system well represents the effects of the bottom topography and therefore provides higher vertical resolution in areas with complex topography. Despite these advantages, models with such a vertical coordinate system have some challenges. Since the vertical layers are tied to the topography, the model is more prone to numerical instability with steep topography. Also, in the areas of flat topography, the model would have relatively low vertical resolutions, which makes it difficult to resolve small-scale features. The major challenge is incorrect diapycnal mixing in the deep ocean occurs where isopycnals cross the vertical coordinates. This inappropriate procedure may prevent the model from restoring in the basin-scale application. To mitigate these problems, applying appropriate stretching parameters and sufficient horizontal and vertical resolutions is important. We adopted the configuration of the ROMS model in Cha et al. 2018, which successfully reproduced the global ocean. The ROMS used in this study was configured globally with a 1° spatial resolution with 30 layers. K-profile parameterization (KPP, Large et al. 1994) is adopted for the vertical mixing scheme widely used in the global ocean under many conditions. (Griffies et al., 2000a). The model was initialized by the climatological World Ocean Atlas (Levitus et al., 2009) and was spun up for 60 years from its initial state using the NCEP/NCAR monthly climatology. Also, the bulk formula (Fairall et al. 1996) was used to parameterize the interaction between the atmospheric-oceanic boundary layer. A detailed configuration of the model was provided in Cha et al. 2018.

The model sea level data along the STCC (from 125E to 260E with a latitude of 21.5~24N) from 1993~2020 was used to compare with the satellite altimetry products.

The results of two ocean reanalysis products, the Hybrid Coordinate Ocean Model (HYCOM;   http://tds.hycom.org/thredds/catalogs/GLBv0.08/expt_53.X.html)   and   Global Reanalysis (GLORYS; https://resources.marine.copernicus.eu/products/), were also examined to confirm the robustness of the Kuroshio intensity in the ECS.

2.6 Ensemble Empirical Mode decomposition (EEMD)

In general, natural processes are non-linear and non-stationary. Thus, it is challenging to get the intrinsic variability in the time series of KVT. To extract the variability of the KVT index with time, we used ensemble empirical mode decomposition (EEMD), which has been widely used in geophysical applications (e.g., Franzke 2010; Ji *et al* 2014; Kidwell *et al.,* 2014; Cha *et al.,* 2021). The EEMD method is based on empirical mode decomposition (EMD), which is designed to decompose arbitrary nonstationary signals into intrinsic mode functions (IMFs) with a long-term adaptive trend, i.e., residue (Huang *et al.,* 1998; Wu and Huang 2008). IMFs are the mathematically complete and nearly orthogonal basis for the original signal having one extreme between zero crossings and a mean value of zero. The EMD breaks down a signal with a shifting process which is as follows (**Figure 3**).

1) Extract all the local maxima and minima of signal X(t).
2) Take the upper and lower envelope determined from a cubic-spline interpolation of the extrema points.
3) Calculate the mean function of the upper and lower envelop, m_1.
4) Let $h_1(t) = X(t) - m_1$. If the mean of $h_1(t)$ is zero, then the shifting process stops,

and h_1 is being a first IMF. If not, $h_1(t)$ is regarded as new data and repeats the above steps until hn satisfies the condition of IMF.

Consequently, the original time series X(t) is equivalent to the sum of IMFs and residue $r(t)$.

$$X(t) = \sum_{i=1}^{n} IMF_i(t) + r(t)$$

Herein, n refers to the number of modes. However, the well-known deficiency of EMD is that intermittent high-frequency waves in the original may interfere with the mode decomposition. Wu and Wang 2009 mitigated this mode mixing problem by adding white noise to the original signal and ensemble average of the results of EMD.

$$C_i = \frac{1}{m} \sum_{j=1}^{m} c_{i,j} \ (i = 1,2,\cdots n, j = 1,2,\cdots m)$$

m is the ensemble number, $c_{i,j}$ is jth IMF of EMD, C_i is ith IMF of the EEMD which ensemble average of $c_{i,j}$ $(i = c, j = 1,2,\cdots m)$. The amplitude of the white noise and ensemble number determined the performance of the EEMD algorithm. If the noise amplitude is too small, it may not resolve the mode mixing problem appropriately. In contrast, too large white noise distorts the original signal and enhances the error. We selected the ensemble number and white noise as 1000 and 0.2 with the reference to Lei et al., 2009).
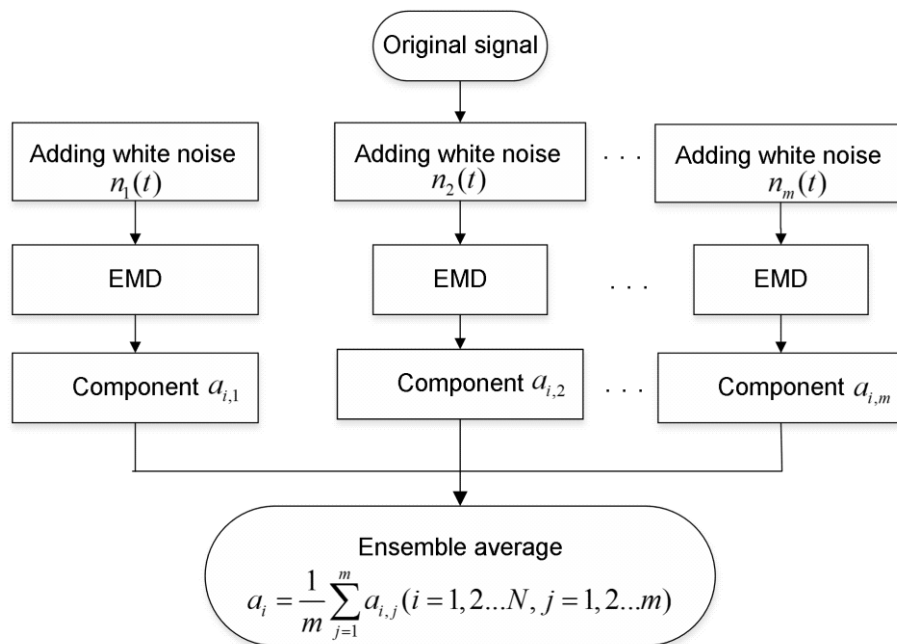
Figure 3. Algorithm of EEMD (Obtained from Park and Choi, 2017)

3. RESULT

As aforementioned, the Kuroshio intensity in ECS is under the effect of EKE in the STCC. In this section, we will examine whether the WSC-induced relationship between the KVT and EKE in STCC persists during the extended period of 1993 to 2020. First, descriptions of estimating KVT in ECS will be presented. Evaluating KVT with proper methods is important because some may provide inaccurate measurements (Yan and Sun 2015). In addition, since the variability of the Kuroshio intensity differs with latitude, local variability can be misinterpreted as dominant variability toward the ECS. Second, the results of previous studies will be reviewed. Several climate indices and changes in the wind pattern over the western North Pacific will be investigated as well as the well-known correlation between EKE in STCC and Kuroshio intensity.

3.1 Interannual variability of Kuroshio intensity in the ECS

The time series of the Kuroshio intensity in ECS, adopting the method suggested by Yan and Sun 2015, is presented in **Figure 4**. The volume transport averaged over 1993–2020 is approximately 20.7 Sv, with a standard deviation of 2.6 Sv, consistent with previous studies (e.g., John *et al.,* 2001; Yan and Sun, 2015; Chang *et al.,* 2015). The power spectrum of the KVT exhibited strong semi-seasonal to annual variability (**Figure 4c**). These high frequencies represent the active mesoscale eddy activities in STCC and their influence on Kuroshio volume transport in East Taiwan. The other distinct frequency is the interannual (5~7 years) signal, which may be associated with the PDO-like wind pattern or low-frequency linear waves. **Figure 4b** shows the low frequency of the KVT, applied two years of moving average to the original time series. After removing high frequency, the empirical estimation of KVT exhibited

a distinct interannual variability in amplitude, with peaks in 1996, 2004, and 2008 and minima in 2000 and 2013. This altimetry-based method has advantages in investigating the modulation by mesoscale phenomena because the east of Taiwan is where oceanic waves frequently collide with the Kuroshio mainstream. However, the variability of Kuroshio intensity east of Taiwan may not last along the shelf break. Especially there is a deep channel in the middle of the Ryukyu Island chain known as Kerama gap. The topographic bridge facilitates the exchanging of water mass between ECS and the western north Pacific. Thus, the variability of ETC may become weak. Utilizing the advantage of EOF that captures the spatial pattern of variability and its changes with time, the most dominant speed variability in the ECS is examined.

The variability of the Kuroshio intensity was also well captured by the first non-seasonal empirical orthogonal function (EOF) mode of the satellite-based surface absolute velocity accounting for 27% of the total variance **Figure 5**. Also, the linear correlation coefficient between the principal component and the estimated KVT reached 0.6 and 0.9 (significantly above the 99% level) for the original and interannual signal, indicating the robustness of the interannual Kuroshio intensity in the ECS. The spatial pattern of the first EOF mode showed that a strong signal occupied the mainstream of the Kuroshio Current along the ECS shelf break, with a maximum in northeast Taiwan (**Figure 5b**). The location of the maximum variability suggests that variability in the east of Taiwan is dominant through the ECS, and the effects of SLAs collides at the East of Taiwan may transfer along the shelf break.

The result of the EOF mode implies that the Kuroshio Current along the shelf break becomes stronger during the positive phase. Thus, the Kuroshio Current in the ECS is characterized by strong interannual variations in the Kuroshio intensity, which strengthen (weaken) when the SLD across the Kuroshio is high (low). The comparison between the empirically estimated KVT and EOF analysis suggests that the interannual mode of the Kuroshio Current reported here is distinctly associated with the SLD across the Kuroshio, resulting in changes in the Kuroshio transport and its intensity along the ECS shelf break.

16

The two reanalysis products of HYCOM and GLORYS also showed an interannual variation in the Kuroshio intensity, which agreed well with the pattern from the altimetry-based datasets (**Figure 6**). Interestingly, the explanation variances of the first EOF modes are higher than that of the altimetry-based dataset. The differences may result from the spatial resolution of the dataset. Since the grids of the OGCMs are twice as dense as the altimetry data, they may have more ability to reproduce and capture SLAs affecting the Kuroshio intensity.
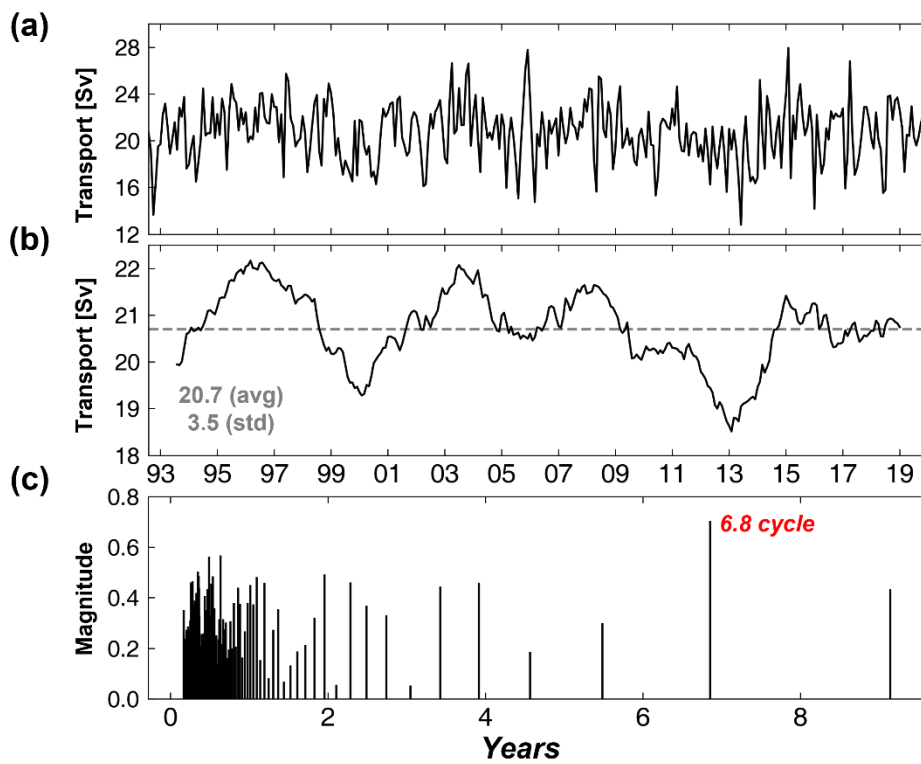
Figure 4. (a) Empirical estimation of Kuroshio volume transport suggested by Yan and Sun 2015. (b) Interannual component of Kuroshio volume transport. (c) Power spectrum of the Kuroshio volume transport in ECS (a).
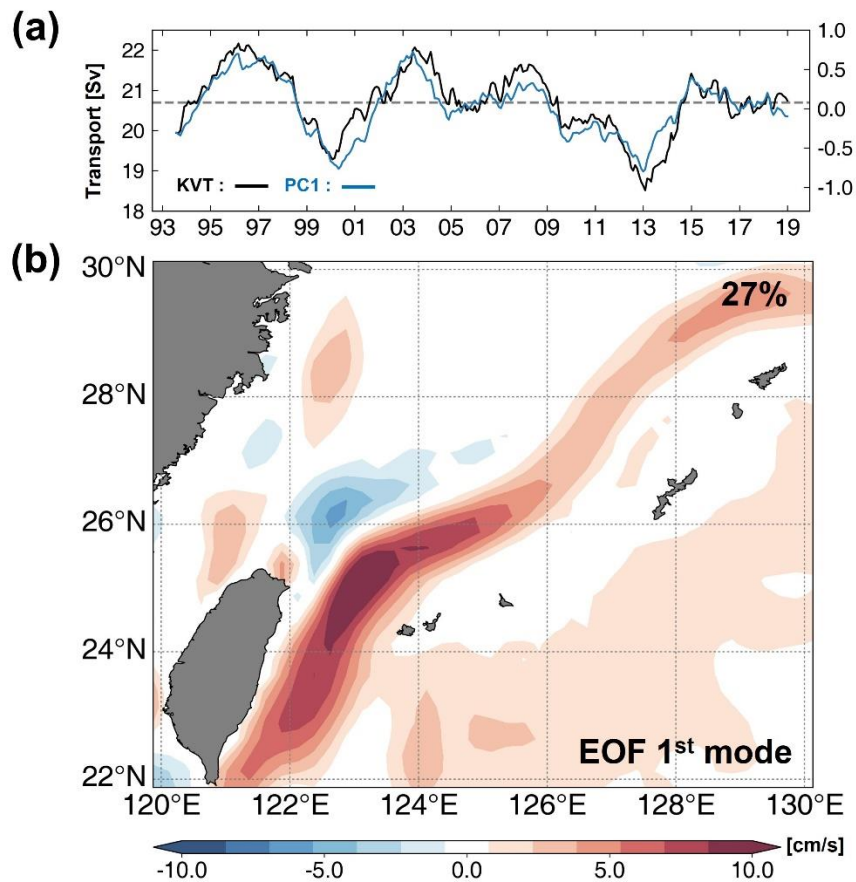
Figure 5. (A) Time series of the monthly KVT (black) and principal component (PC) of first mode for satellite-based surface velocity (blue) over 1993–2020. Two-year moving average was applied to both KVT and PC time series. Grey dashed line indicates the average of the KVT (20.7Sv) over the period. **(B)** Spatial pattern of first-leading mode of geostrophic velocity in the ECS region.
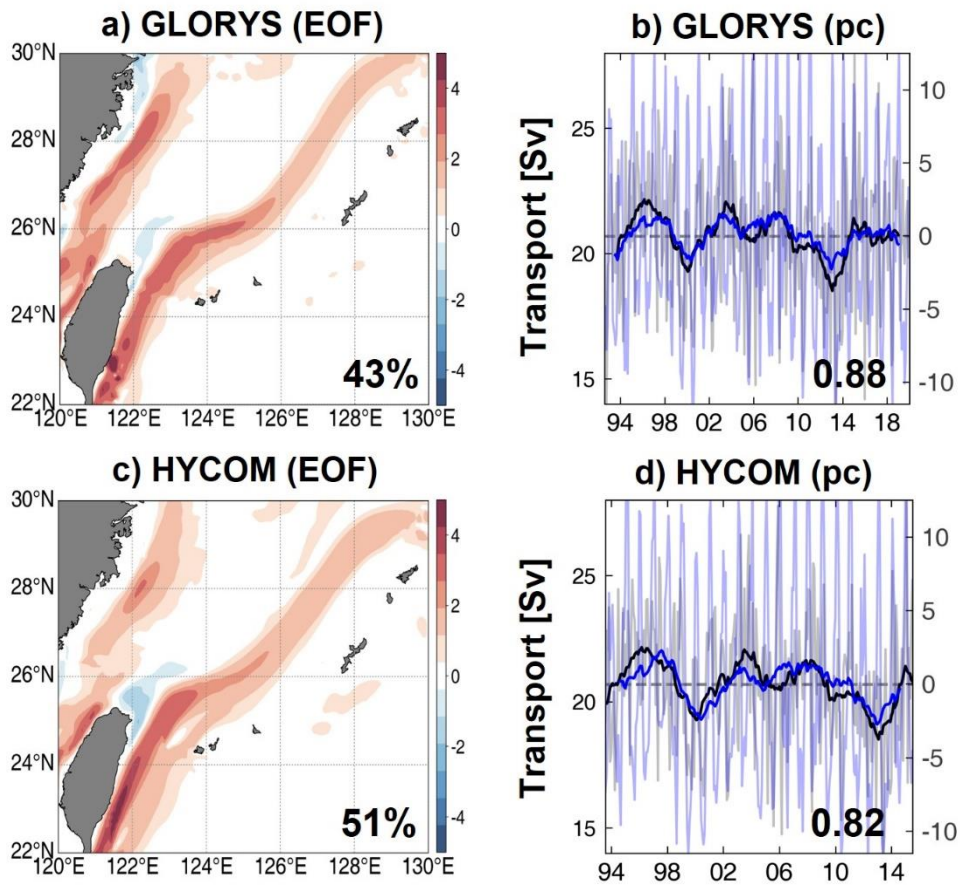
Figure 6. Spatial pattern of first-leading mode of surface speed in the ECS depicted from (a) GLORYS, during 1993-2020 and (c) HYCOM during 1994–2014. Corresponding pc time series (blue) of GLORYS (b) and HYCOM (d) and their two years running average (thick blue line).

In addition, the composite analysis for SLAs sorted according to the phase of the low-pass filtered KVT further supported the interannual fluctuation of ECS-Kuroshio, showing high (low) SLD across the Kuroshio during periods of strong (weak) KVT (**Figure 7**).

An interesting feature is that the strongest SLA signals were mainly detected in eastern Taiwan, extending eastward along the latitude band of 20–23°N. This SLA pattern corresponds to the region with abundant eddies, which is called the eddy zone (Qiu 1999; Chelton *et al.,* 2011). These results demonstrate the robust interannual variability of the Kuroshio intensity in the ECS, which may be associated with SLAs propagating from the interior ocean, such as mesoscale eddy migrations (Chang *et al.,* 2015; Chang and Oey 2011).

Figure 7. Composite maps of SLAs during the positive **(A)** and negative **(B)** periods of the KVT east of Taiwan. The positive (negative) period is referred to when the Kuroshio intensity (black line of Figure 1A) is above (below) the average.

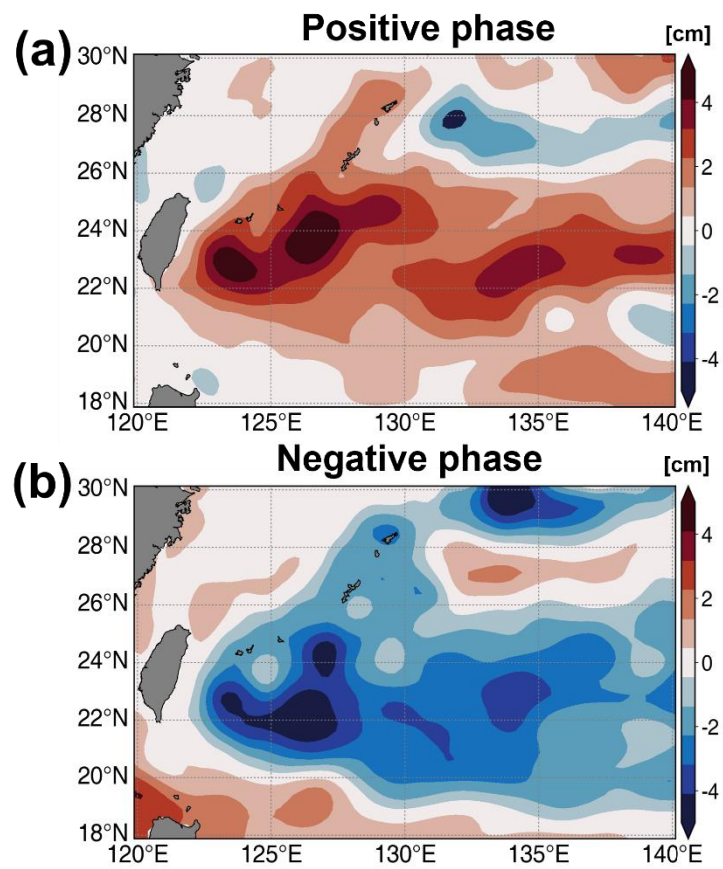## 3.2 Kuroshio intensity associated with mesoscale eddy activities

Several studies have shown that Kuroshio transport can be influenced by westward-propagating eddies generated in the STCC, colliding with the east coast of Taiwan (Chang *et al.,* 2015). The generation of the mesoscale eddies is closely related to baroclinity in the ocean which indicates how the misaligned pressure gradient is from the density gradient. Interaction between the eastward STCC and westward NEC in the subsurface layer produces baroclinic instability in STCC (Qiu and Chen 2010; Qiu and Chen 2013; Chang and Oey 2012; Chang and Oey 2014). The baroclinic instability in STCC is modulated by atmospheric conditions over the western north pacific. In the interannual time scale, the PDO-related WSC pattern fluctuates with a positive peak on the east side of Taiwan and a negative peak on the east side of the Philippines. The see-saw-like WSC pattern induces meridional thermocline tilt by strengthening the southward Ekman flux forcing. Thus, during the positive phase of PDO, EKE increases, followed by enhanced baroclinic instability in STCC. In contrast, negative PDO relaxes the density slope gradient and decreases EKE in STCC. Wind patterns over the NEC-STCC system can thus provide favorable conditions for the generation of eddies by changing the EKE owing to baroclinic instability. Qiu and Chen (2013) showed the interannual to decadal variability of the EKE in the STCC, which is related to the PDO-like large-scale WSC pattern. Qiu and Chen (2013) showed the interannual to decadal variability of the EKE in the STCC, which is related to the PDO-like large-scale WSC pattern. Hsin *et al.,* (2013) also reported a correlation between the KVT east of Taiwan and the PDO index.

To identify the relationship between Kuroshio and PDO-related eddy activities, we compared the KVT east of Taiwan with the EKE over the STCC and the PDO index on an interannual time scale (**Figure 8**). During 1993–2003, the EKE and PDO indices were well correlated with the KVT east of Taiwan with correlation coefficients of 0.82 and 0.91,

respectively. These high positive correlations provide strong support for the results of previous studies that indicated that PDO-like wind patterns and subsequent eddy activities in the STCC can modulate the interannual KVT east of Taiwan (Hsin *et al.,* 2013).

However, the correlation coefficients have decreased markedly over the past decade, down to 0.23 and 0.5, respectively, disagreeing with the mechanism proposed by the above-mentioned studies. This disagreement is also evident from the correlation patterns between the KVT east of Taiwan and the WSC over the western North Pacific (0–30°N, 120–170°W) on an interannual timescale (**Figure 9**). Before the early 2000s, the dominant correlation pattern was a strong north–south dipole in the western North Pacific, with a positive correlation in the NEC region and a negative correlation in the STCC region, similar to the PDO pattern (**Figure 10**). This PDO-related wind pattern plays an important role in determining the mesoscale eddy activities in the STCC owing to the baroclinic instability of the NEC–STCC system (Qiu and Chen 2013). In contrast, the dipole WSC pattern has not persisted since the early 2000s, disagreeing with the mechanism proposed by previous studies that indicated that the Kuroshio intensity could be modulated by PDO-related eddy activities in the STCC and their migration to the west. The NCEP/NCAR reanalysis-1 also showed a similar pattern (**Figure 10**).

To further clarify the effect of mesoscale eddies on the KVT east of Taiwan, EOF analysis was conducted on the temporally varying EKE on an interannual timescale (**Figure 11**). The spatial pattern of the first EOF mode mainly corresponds to mesoscale structures in the region east of Taiwan (**Figure 11a**). This mode is associated with SLAs, which reflect mesoscale eddies that propagate from the STCC region. The principal time series was highly correlated with the KVT east of Taiwan before 2003 (r = 0.8, significance above the 99% confidence level), indicating that the migration of eddies modulated the Kuroshio intensity along the ECS on an interannual timescale (**Figure 11b**). This result further supports the results of Chang and Oey (2011). However, the strong relationship between the Kuroshio intensity and eddies has

decreased since 2003, showing a poor correlation coefficient of 0.01. The correlation maps between the time series of the EKE east of Taiwan and the low-pass filtered SLAs in the western North Pacific further confirm the change in the response of the SLAs to eddy activity in the region east of Taiwan (**Figure 12**). Prior to the early 2000s, the EKE east of Taiwan was positively correlated with SLAs, showing a tilted band structure extending from the east of Taiwan to approximately 145°E. This pattern is consistent with the eddy zone in the STCC, but a different correlation pattern appeared after the early 2000s. High correlations were observed in the central and eastern North Pacific, gradually decreasing towards the west along the zonal bands. These results confirm that the influence of the eddy activity east of Taiwan on the interannual Kuroshio intensity has weakened since the early 2000s. Thus, the poor correlation suggests that the mesoscale eddy activities in the STCC region and their arrival on the east coast of Taiwan are no longer the dominant factors that modulate the interannual Kuroshio intensity along the ECS.
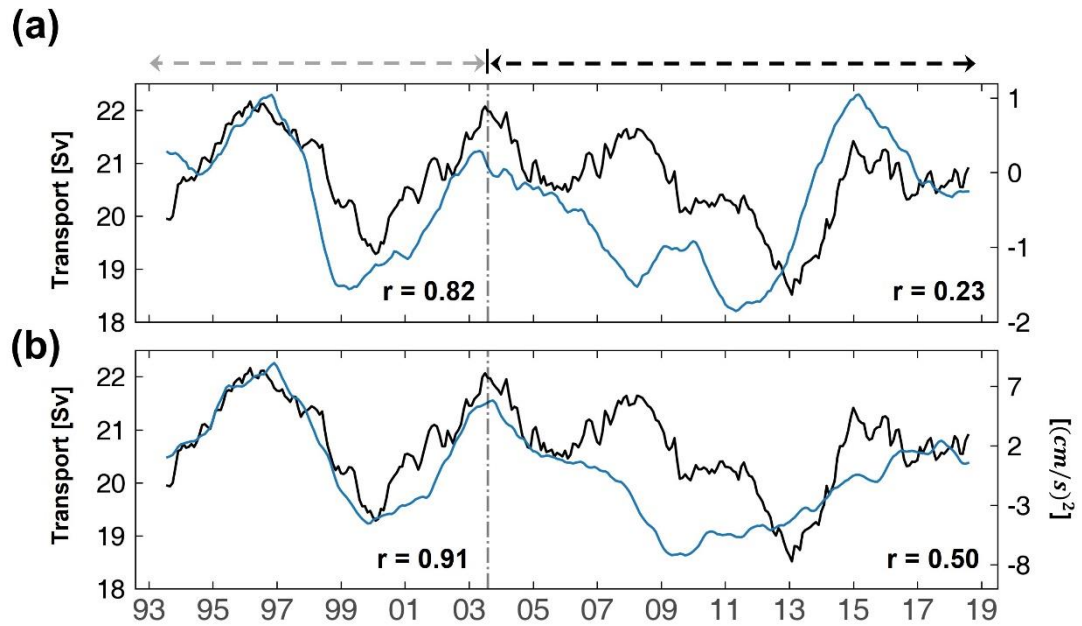
Figure 8. Comparison of the KVT east of Taiwan (black) time series with **(A)** PDO index (blue) and **(B)** EKE index (blue) averaged over the STCC region (10°–30°N, 125°–110°W) in the western North Pacific. The correlation coefficients are computed for two periods: before and after 2003 (vertical grey dashed lines).
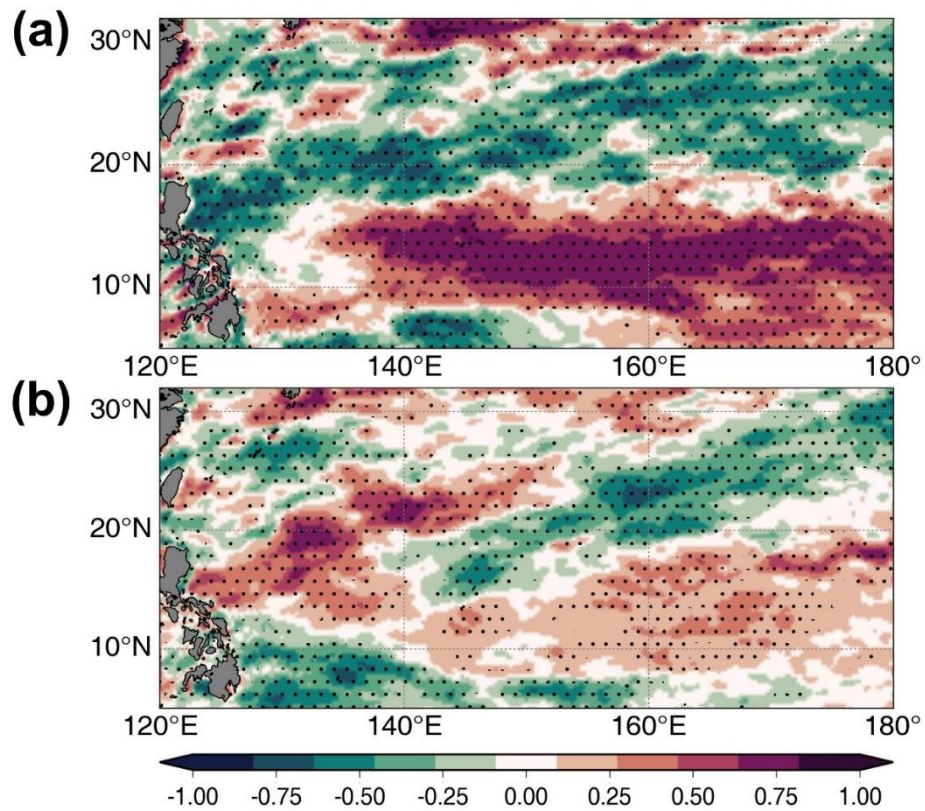
Figure 9. Correlation maps of wind stress curl (WSC) over the western North Pacific with the KVT east of Taiwan during the periods of **(A)** 1993–2003 and **(B)** 2004–2019. Two-year moving average was applied to the WSC data. Dotted areas denote the significance level above 99%.
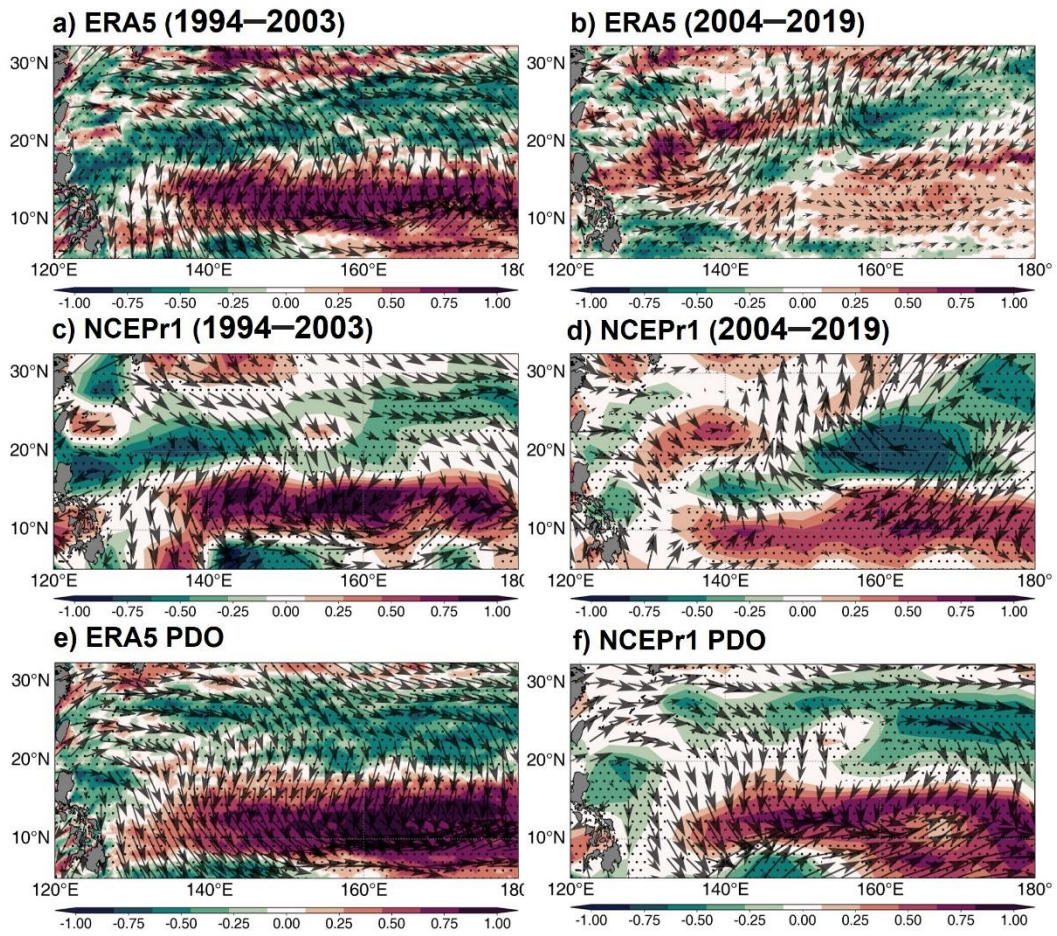
Figure 10. Correlation maps of wind stress curl (WSC) and Wind vector of the ERA5 and NCEPr1 over the western North Pacific with the KVT during the periods of (a) (c) 1993–2003, (b) (d) 2004–2019. Correlation map of WSC and Wind vector with the PDO index in whole research periods (1994–2019). Two-year moving average was applied to the WSC data. Dotted areas denote the significance level above 99%.
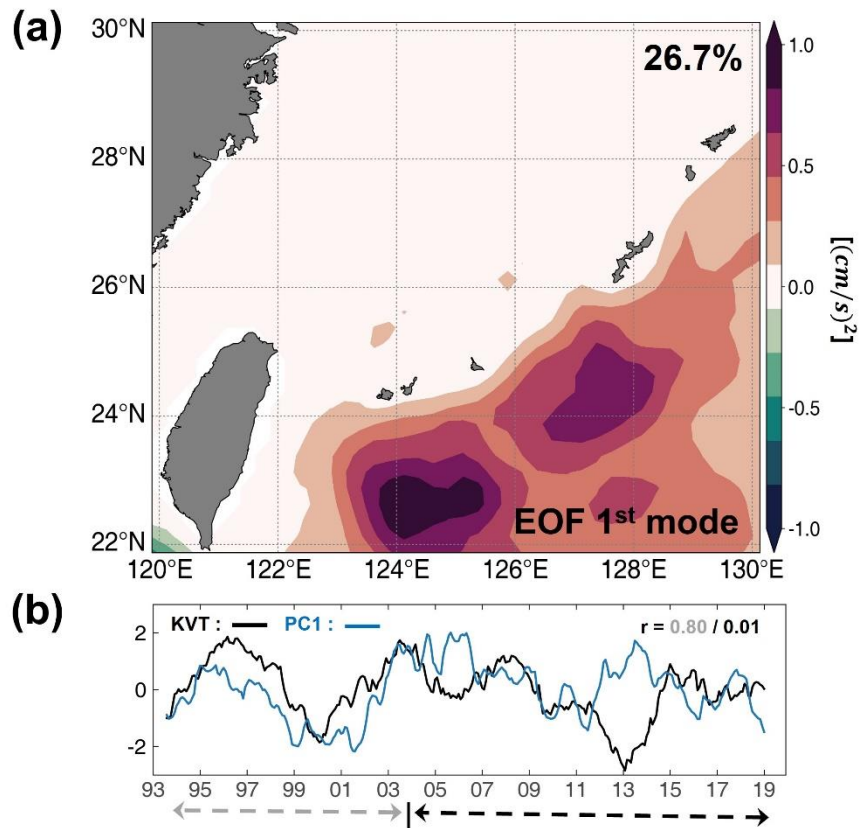
Figure 11. (A) Spatial pattern of the EOF first leading mode of the EKE in the east of Taiwan, which accounts for 26.7% of the total variance. **(B)** Time series of the KVT east of Taiwan (black) and the PC (blue) of the leading mode. Both time series were smoothed by two-year moving average. The correlation coefficients are computed for two periods: before and after 2003.

Figure 12. Correlation maps of SLAs with the EKE index during the periods of **(A)** 1993–2003 and **(B)** 2004–2019.

3.3 SLAs propagating westward from central and eastern North Pacific

As aforementioned, the interannual KVT in the ECS is determined by the SLD across the Kuroshio Current, which can be changed by SLAs east of Taiwan. To identify the SLA responses to the Kuroshio intensity, we computed the composite mean SLAs according to the strong (1995–1998 and 2006–2009) and weak (1999–2002 and 2012–2014) pe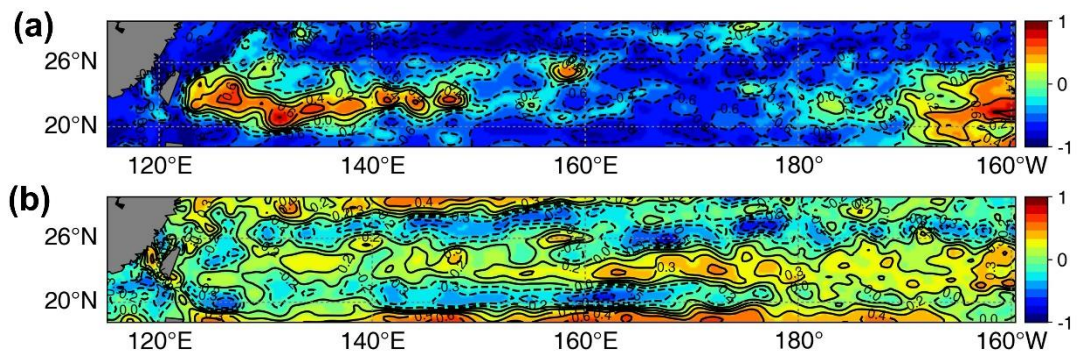riods of the KVT on an interannual time scale (**Figure 13**). As expected, the results showed that a high (low) SLA persisted in eastern Taiwan at times when the KVT was strong (weak). However, the spatial patterns of SLAs according to the phase of the KVT were quite different before and after the early 2000s. Before 2003, strong positive and negative SLAs were confined only from the east of Taiwan to approximately 145°E along the latitude band of 20–23°N, consistent with the eddy zone in the STCC region (**Figure 13 a,b**). However, after the early 2000s, the SLAs were characterized by a zonally elongated band structure extending from the east coast of Taiwan to the central and eastern North Pacific (**Figure 13 c,d**). These SLA patterns further support our results, indicating that the interannual variability of Kuroshio intensity was mainly modulated by the migration of eddies from the STCC region until the early 2000s but that their relationship no longer holds since then.

Our analysis suggests that over the past three decades, the Kuroshio intensity has been influenced by not only eddy activities but also other modes on an interannual time scale. To capture the dominant modes of the KVT east of Taiwan, we used the EEMD method, which is designed to separate the original time series into several IMFs and a residual trend (Huang *et al.,* 1998; Wu and Huang 2009). The EEMD results yielded seven IMFs and residues in ascending order from high to low frequencies (**Figure 14**), which above significant level 99% except for IMF7 (**Figure 15**). Distinct interannual and subdecadal fluctuations with peak periods of ~3 and ~7 years, respectively, were identified in the KVT east of Taiwan, which can explain most of the interannual variability in the Kuroshio intensity over the past three decades (**Figure 16a,b**). Notably, these two modes clearly represent different spatial patterns of SLAs,

제주대학교 중앙도서관
JEJU NATIONAL UNIVERSITY LIBRARY

as shown in the SLA regression with regard to the interannual and subdecadal modes (**Figure 16c,d**). The EEMD-determined interannual mode exhibited a spatial pattern of mesoscale eddy activity confined to the STCC eddy zone, similar to the pattern of the composite mean SLAs before the early 2000s (see **Figure 13a,b**). This mode, associated with westward-migrating eddies from the STCC region, explains the interannual modulation of the KVT east of Taiwan until the early 2000s, consistent with the findings of Soeyanto *et al.,* (2014). In contrast, the regression map of SLA for the subdecadal mode represents the zonally elongated band at 20–23°N, which may be linked to the westward propagation of oceanic planetary waves from the central and eastern North Pacific. Unlike the interannual eddy mode, the subdecadal mode became stronger in amplitude after the early 2000s, indicating that the low-frequency variability contributed more to modulating the ECS-Kuroshio intensity through westward-propagating SLAs. To identify the surface wind patterns associated with these modes, we have projected the wind stress pattern in the Pacific upon the interannual and subdecadal modes by a linear regression approach (**Figure 17**). The interannual mode corresponds to wind patterns at mid-and high latitudes (north of 40°N) in the North Pacific, describing a large amplitude oscillation (Figure 9A). This pattern resembles the general pattern of PDO, showing consistency with our finding that the interannual KVT mode is linked to the PDO-related mesoscale eddy activities in the STCC region. On the other hand, the subdecadal mode is mainly driven by strong wind oscillation centered at 30°N in the central/eastern North Pacific (**Figure 17b**), which is different from the PDO-related wind pattern. A recent study by Wu *et al.* (2019) found that the Pacific climate conditions favored the North Pacific Gyre Oscillation-like pattern since 1999 to replace the PDO, thereby showing significant variability over the central/eastern Pacific. This alternation of wind pattern since late 1990s probably contributes to low-frequency SLAs that propagate westward across the North Pacific.

The Hovmöller diagram of SLA along the 21.5–24°N band further supports the westward propagation of SLAs that modulate the KVT east of Taiwan (**Figure 18**). Prior to the early

2000s, the westward-propagating low and high SLAs were confined to the eddy zone in the STCC region. Since then, they have slowly traveled a long across the Pacific Basin, identified as the baroclinic Rossby waves. Assuming a propagation speed of approximately 5.5 cm s^{-1} in the latitude band of 22–24°N, the baroclinic waves take approximately 6.4 years to travel a distance of 110,000 km from the eastern boundary to the east coast of Taiwan (Chelton and Schlax 1996; Andres *et al.,* 2011). This is similar to the propagation speed estimated from the observed SLAs. Although satellite altimetry products may represent that the interannual variability of the Kuroshio intensity in the ECS had been related to mesoscale processes, it cannot reveal how specific oceanic phenomena have modulated the Kuroshio intensity over the past three decades. Since oceanic mesoscale eddies can only be resolved with a high-resolution ocean general circulation model (OGCM), a coarse Regional Ocean Modeling System (ROMS) was adopted to split the effect of mesoscale eddies and other oceanic phenomena. To confirm the influence of wave propagation from the east on the modulation of the KVT, we also used the result of an OGCM, whose dynamic is dominated by wind-forced Rossby waves and Sverdrup balance. Notes that because the horizontal resolution is 1°, eddy activities generated by shear instability in the STCC region are not resolved in the OGCM (**Figure 18c**). Prior to early 2000s, the observed and modeled KVT east of Taiwan do not correlate well, suggesting that the model dynamics without mesoscale eddy generation are not dominant in producing the observed SLAs east of Taiwan. However, since 2000s the model result shows similar SLAs that propagated westward across the North Pacific as those from the altimeter. As expected, the ocean model fairly reproduced the westward-propagating SLAs from the east although their magnitude and speed were slightly weak and slow compared to those from the observation. The model-data comparison demonstrates that the observed SLAs east of Taiwan are influenced by both the mesoscale eddy activities and the westward propagation of wind-forced waves over the past three decades. This result is consistent with previous studies showing that the westward propagation of oceanic Rossby waves is linked to

the modulation of Kuroshio intensity in the ECS (Andres *et al.,* 2011; Wu *et al.,* 2019). Using the extended records of the SLA dataset until 2020, our results clarify that the interannual modulation of the Kuroshio intensity in the ECS is determined by a combination of two dominant modes: mesoscale eddy activities in the STCC driven by PDO-related oceanic instability (Qiu and Chen 2013; Qiu and Chen 2014) and low-frequency planetary waves traveling westward across the Pacific Basin (Fu and Qiu 2002; Andres *et al.,* 2011). These two modes contributed differently, depending on the time period, to the modulation of the ECS-Kuroshio intensity. Eddy activities in the STCC region have thus consistently fluctuated over the past three decades, whereas the low-frequency mode has strengthened since the early 2000s, thereby modulating the interannual variability of the Kuroshio intensity in the ECS.
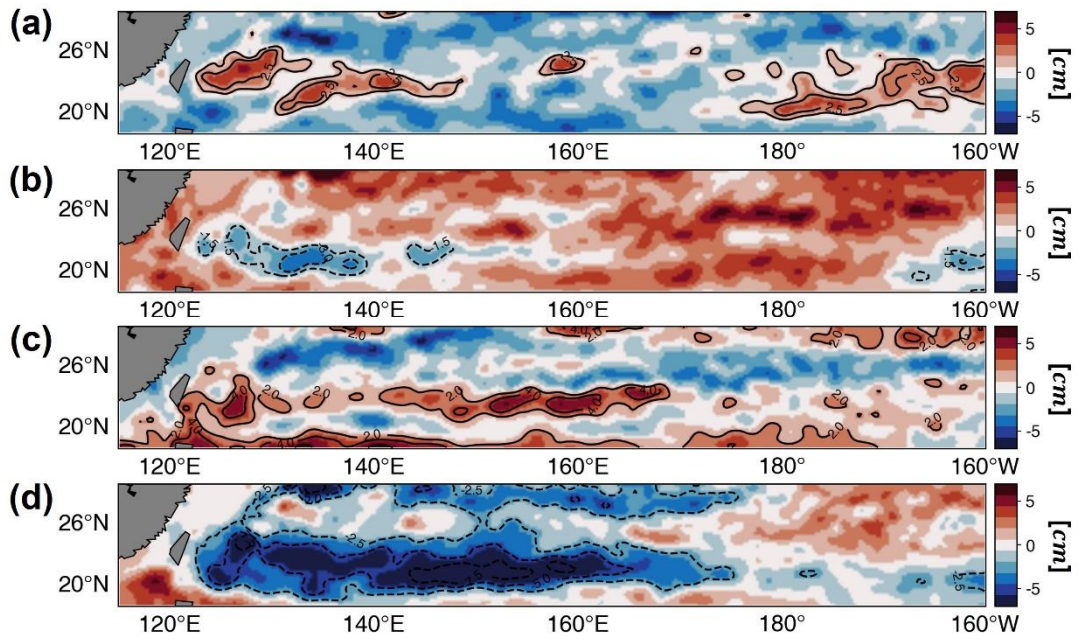
Figure 13. Composite maps of SLAs according to strong years of **(A)** 1995–1998 and **(C)** 1999–2002 and weak years of **(B)** 2006–2009 and **(D)** 2012–2014 on the KVT east of Taiwan.
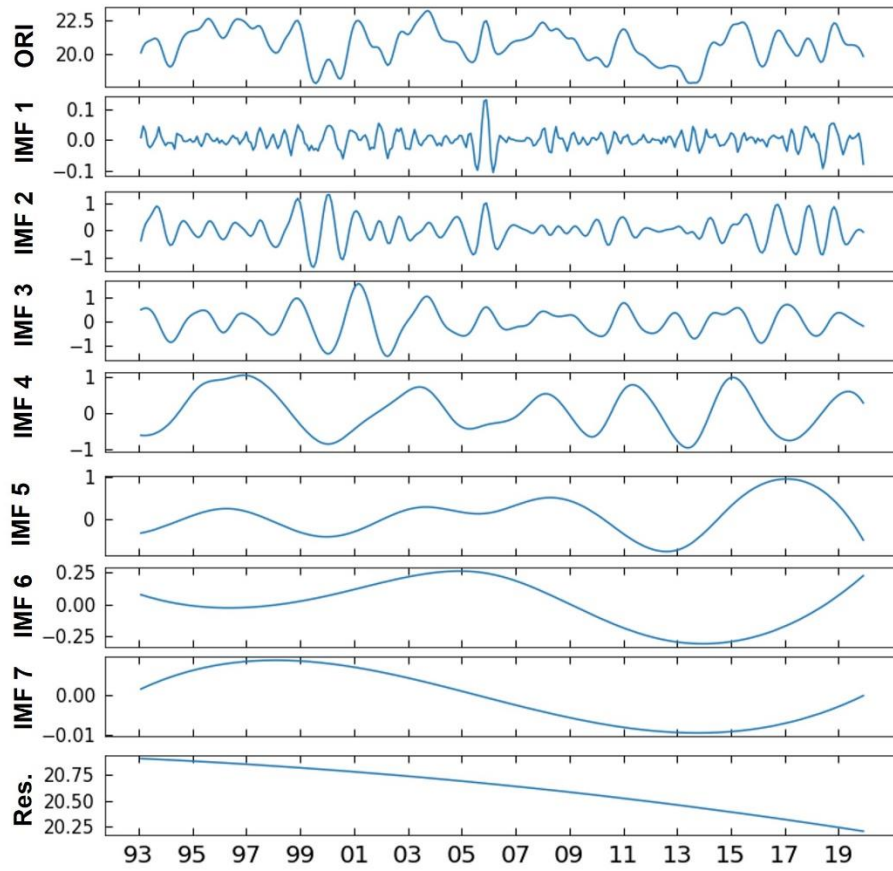
Figure 14. EEMD decompositions of one year low-pass filtered KVT. The original monthly data (top) are decomposed into seven IMFs and the resulting trends (bottom panels) by EEMD method.
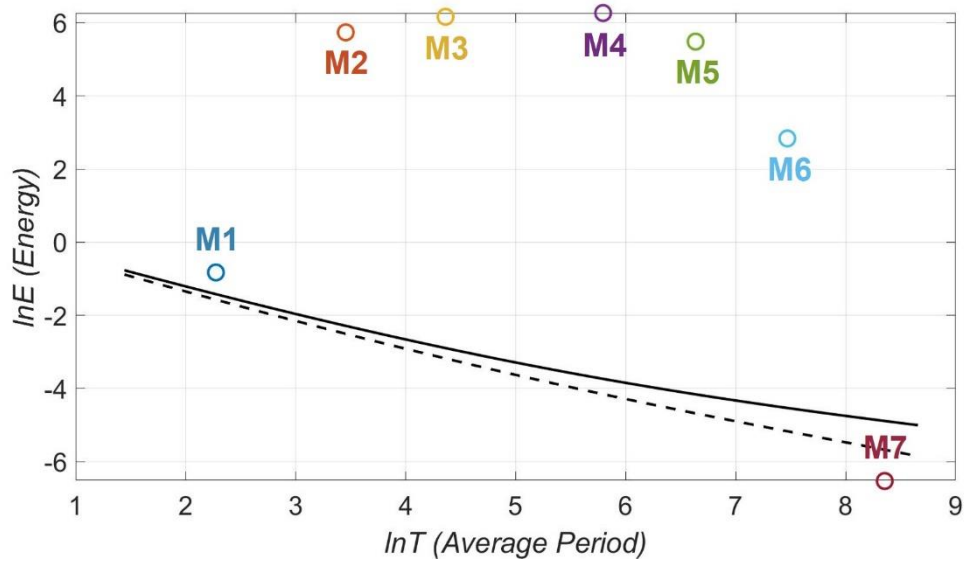
Figure 15. Statistical significance tests of the seven IMFs of the KVT. The dashed lines represent the 95% confidence level, and the solid lines are the 99% confidence level. Except for IMF7, all IMFs are distinguishable from Gaussian white noise at both confidence levels.
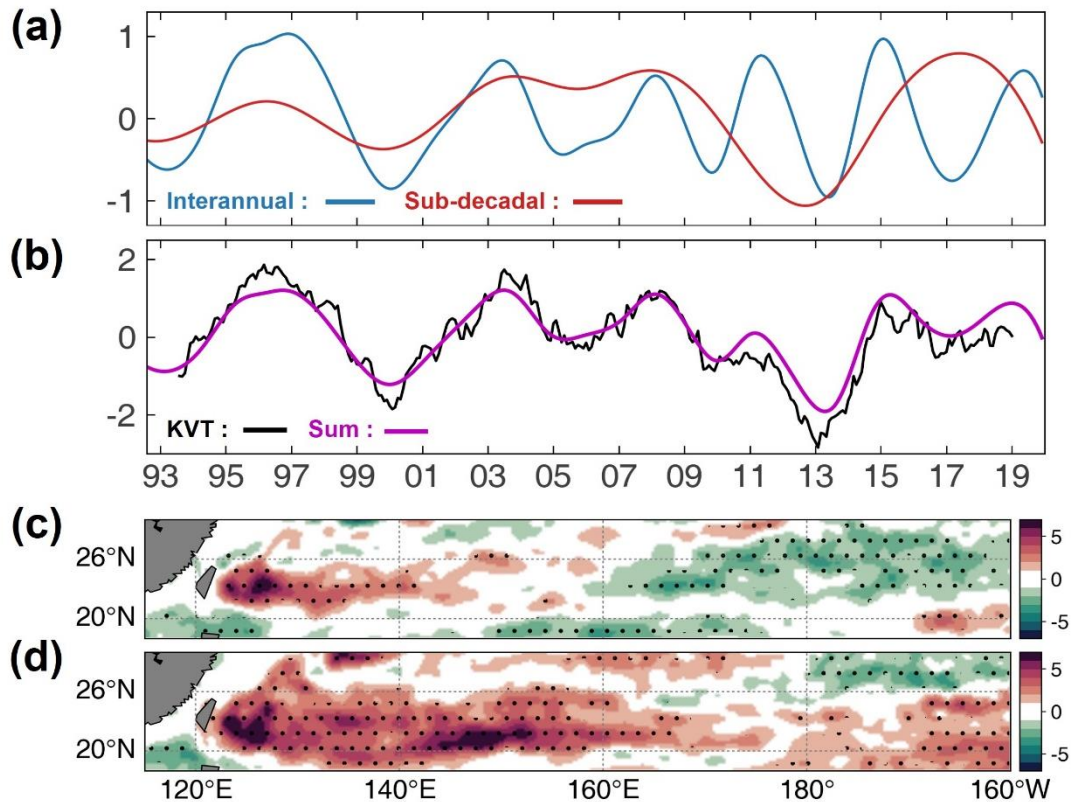
Figure 16. (A) Interannual (red) and sub-decadal (blue) modes of the KVT east of Taiwan extracted by EEMD method from 12-month low-passed filtered KVT time series. **(B)** Time series of the KVT east of Taiwan (black) and the sum of EEMD-determined two modes (purple) in **(A)**. Two time series are normalized by their standard deviation. Regression maps of SLAs against **(C)** the interannual and **(D)** sub-decadal mode over the period of 1993–2020. Dotted areas represent the significance level above 95%.
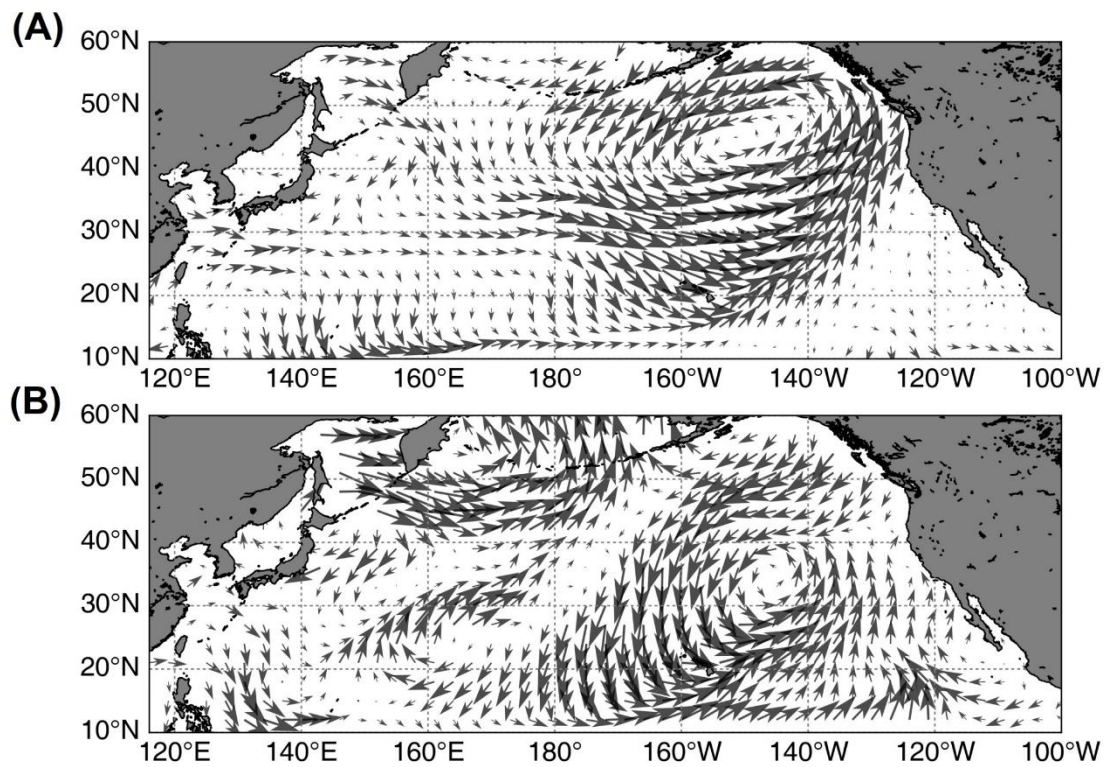
Figure 17. Regression maps of wind vectors against **(A)** the interannual and **(B)** sub-decadal mode over the period of 1993–2020. Two-year moving average was applied to the wind vectors of each grid point before regression.
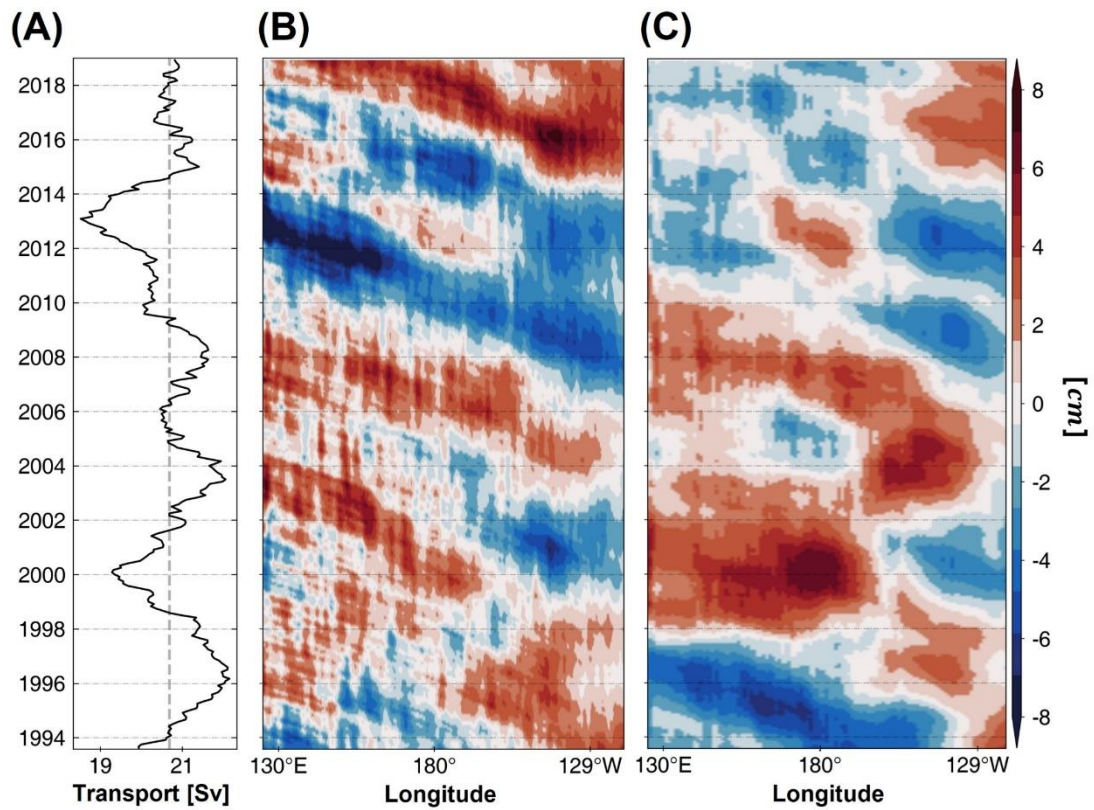
Figure 18. (A) Interannual variation of the KVT east of Taiwan over the period of 1994–2019 and Hovmöller diagram of the SLA of the **(B)** altimeters and **(C)** OGCM result along the latitude band of 21.5–24°N. Two-year moving average was applied to the data. Grey dashed line represents the mean value of the KVT east of Taiwan over the period.

4. CONCLUSION

Understanding the changes in the ECS-Kuroshio intensity can provide important information on the ocean's role in modulating the regional climate system. In this study, we conducted observational analyses to investigate Kuroshio intensity in the ECS and its modulation on an interannual timescale. The extended record of SLAs exhibited a distinct interannual variability of the ECS-Kuroshio intensity, which is positively correlated with mesoscale eddy activities in the STCC region and provides observational support for previous studies, indicating the important role played by mesoscale eddies associated with baroclinic instability in the STCC region. However, the interannual variation of the Kuroshio intensity no longer had a strong positive correlation with eddy activities after the early 2000s. Our analysis showed that the interannual modulation of Kuroshio intensity can be determined by a combination of westward-propagating mesoscale eddies from the STCC region and oceanic planetary waves from the east. The analysis using the EEMD method demonstrated that eddy activities in the STCC region have fluctuated consistently over the past three decades, whereas the low-frequency mode has become stronger since the early 2000s, thereby modulating the interannual variability of the Kuroshio intensity. Consequently, prior to the early 2000s, the interannual variability of the Kuroshio was mainly affected by the formation and propagation of eddies from the STCC region, associated with oceanic instability in the STCC-NCE system. However, since then, low-frequency waves propagating westward across the Pacific Basin have largely modulated the Kuroshio variability in the ECS by superimposing the variability associated with eddy activities.

Unlike mesoscale eddy activities, low-frequency variability has become stronger since the early 2000s, coinciding with the recent global warming hiatus. Several studies have reported that during the hiatus period, the western Pacific experienced remarkable decade-long shifts in atmospheric and oceanic circulation (e.g., England *et al.,* 2014; Wang *et al.,* 2016; Cha *et*

al., 2018; Wang and Wu 2019). Although not the focus of this study, the low-frequency mode in the ECS-Kuroshio intensity may be linked to the decadal shift in the Pacific climate during the warming hiatus. This study may thus have implications on the decadal prediction of Kuroshio intensity in the ECS, which remains a challenging issue.

References

Andres, M., Kwon, Y.-O., and Yang, J. (2011) Observations of the Kuroshio's barotropic and baroclinic responses to basin-wide wind forcing. *J. Geophys. Res. Oceans* 116. doi: 10.1029/2010JC006863

Cha, S. C., Moon, J. H., and Song, Y. T. (2018) A Recent Shift Toward an El Niño-Like Ocean State in the Tropical Pacific and the Resumption of Ocean Warming. *Geophys. Res. Lett. 45,* 11,885-11,894. doi: 10.1029/2018GL080651

Cha, H., Moon, J. H., Kim, T. K., and Song, Y. T. (2021) Underlying drivers of decade-long fluctuation in the global mean sea-level rise. *Environ. Res. Lett.*16, 124064.

Chelton, D. B., and Schlax, M. G. (1996) Global Observations of Oceanic Rossby Waves. *Science* 272, 234–238. doi: 10.1126/science.272.5259.234

Chelton, D. B., Schalax, M. G., and Samelson, R. M. (2011) Global observation of nonlinear mesoscale eddies. *Prog. Oceanogr.* 91, 167–217. doi: 10.1016/j.pocean.2011.01.002

Chang, M.-H., Jan, S., Mensah, V., Andres, M., Rainville, L., Yang, Y.J., Cheng, Y.-H., (2018) Zonal migration and transport variations of the Kuroshio East of Taiwan induced by eddy impingements. Deep Sea Research Part I: Oceanographic Research Papers 131, 1–15. doi:10.1016/j.dsr.2017.11.006

Chang, Y. L., and Oey, L. Y. (2011) Interannual and seasonal variations of Kuroshio transport east of Taiwan inferred from 29 years of tide-gauge data. *Geophys. Res. Lett.* 38. doi: 10.1029/2011GL047062

Chang, Y. L., and Oey, L. Y. (2012) The Philippines–Taiwan Oscillation: Monsoonlike Interannual Oscillation of the Subtropical–Tropical Western North Pacific Wind

System and Its Impact on the Ocean**. *J. Climate*. 25 1597-1618. doi: 10.1175/JCLI-D-11-00158.1

Chang, Y. L., and Oey, L. Y. (2014) Instability of the North Pacific Subtropical Countercurrent. *J. Phys. Oceanogr.* 44, 818–833. doi: 10.1175/JPO-D-13-0162.1

Chang, Y. L., Miyazawa, Y., and Guo, X. (2015) Effects of the STCC eddies on the Kuroshio based on the 20-year JCOPE2 reanalysis results. *Prog. Oceanogr*. 135, 64–76. doi: 10.1016/j.pocean.2015.04.006

Gan, M., Kwon, Y.-O., Joyce, T. M., Chen, K., and Wu, L. (2019) Influence of the Kuroshio Interannual Variability on the Summertime Precipitation over the East China Sea and Adjacent Area. *J. Climate* 32, 2185–2205. doi: 10.1175/JCLI-D-18-0538.1

England, M. H., McGregor, S., Spence, P., Meehl, G. A., Timmermann, A., Cai, W., Gupta, A. S., McPhaden, M. J., Purich, A., and Santoso, A. (2014) Recent intensification of wind-driven circulation in the Pacific and the ongoing warming hiatus. *Nature Clim. Change* 4, 222–227.

Franzke, C. (2010) Long-Range Dependence and Climate Noise Characteristics of Antarctic Temperature Data. *J. Climate* 23, 6074–6081. doi: 10.1175/2010JCLI3654.1

Fu, L. L., and Qiu, B. (2002) Low-frequency variability of the North Pacific Ocean: The roles of boundary- and wind-driven baroclinic Rossby waves. *J. Geophys. Res. Oceans* 107, 13–1–13–10.

Hsin, Y. C., Chiang, T. L., and Wu, C. R. (2011) Fluctuations of the thermal fronts off northeastern Taiwan. *J. Geophys. Res. Oceans* 116. doi: 10.1029/2011JC007066

Hsin, Y. C., Qiu, B., Chiang, T. L., and Wu, C. R. (2013) Seasonal to interannual variations in the intensity and central position of the surface Kuroshio east of Taiwan. *J. Geophys. Res. Oceans* 118, 4305–4316. doi: 10.1002/jgrc.20323

Huang, N. E., Shen, Z., Long, S. R., Wu, M. C., Shih, H. H., Zheng, Q., Yen, N.-C., Tung, C. C., and Liu, H., H. (1998) The empirical mode decomposition and the Hilbert spectrum for nonlinear and non-stationary time series analysis. *Proc. R. Soc. A. 454, 903-95. doi:* 10.1098/rspa.1998.0193

Huang, N. E., and Wu, Z. (2008) A review on Hilbert-Huang transform: method and its applications to geophysical studies. *Rev. Geophys. 46, doi:* 10.1029/2007RG000228

Johns, W. E., Lee, T. N., Zhang, D., Zantopp, R. J., Liu, C. T., and Yang, Y. (2001) The Kuroshio East of Taiwan: Moored Transport Observations from the WOCE PCM-1 Array. *J. Phys. Oceanogr.* 31, 1031–1053. doi: 10.1175/1520-0485(2001)031<1031:TKEOTM>2.0.CO;2

Ji, F., Wu, Z., Huang, J., and Chassignet, E. P. (2014) Evolution of land surface air temperature trend. *Nature Clim. Change* 4, 462–466.

Jo, S., Moon, J.-H., Kim, T., Song, Y., and Cha H. (2022) Interannual Modulation of Kuroshio in the East China Sea Over the Past Three Decades. *Front. Mar. Sci.* 9:909349. doi: 10.3389/fmars.2022.909349

Kidwell, A., Jo, Y. H., and Yan, X. H. (2014) A closer look at the central Pacific El Niño and warm pool migration events from 1982 to 2011. *J. Geophys. Res. Oceans* 119, 165–172. doi: 10.1002/2013JC009083

Lien, R. C., Ma, B., Cheng, Y. H., Ho, C. R., Qiu, B., Lee, C. M., and Chang, M. H. (2014) Modulation of Kuroshio transport by mesoscale eddies at the Luzon Strait entrance. *J. Geophys. Res. Oceans* 119, 2129–2142. doi: 10.1002/2013JC009548

Lien, R. C., Ma, B., Lee, C. M., Sanford, T. B., Mensah, V., Centurioni, L. R., Cornuelle, B. D., Gopalakrishnan, G., Gordon, A. L., Chang, M. H., Jayne, S. R., and Yang, Y. J. (2015) The Kuroshio and Luzon Undercurrent East of Luzon Island, *Oceanography* 28, 54–63.

doi: 10.5670/oceanog.2015.81

Maher, N., Gupta, A. S., and England, M. H. (2014) Drivers of decadal hiatus periods in the 20th and 21st Centuries. *J. Geophys. Res*. 41, 5978–5986. doi: 10.1002/2014GL060527

Nakamura, H., Nishina, A., Tobata, K., Higashi, M., Habano, A., and Yamashiro, T. (2012) Surface velocity time series derived from satellite altimetry data in a section across the Kuroshio southwest of Kyushu. *J. Oceanogr.* 68, 321–336.

Qiu, B. (1999) Seasonal Eddy Field Modulation of the North Pacific Subtropical Countercurrent: TOPEX/Poseidon Observations and Theory. *J. Phys. Oceanogr.* 29, 2471–2486. doi: 10.1175/1520-0485(1999)029<2471:SEFMOT>2.0.CO;2

Qiu, B., and Chen, S. (2010) Interannual Variability of the North Pacific Subtropical Countercurrent and Its Associated Mesoscale Eddy Field. *J. Phys. Oceanogr.* 40, 213–225. doi: doi.org/10.1175/2009JPO4285.1

Qiu, B., and Chen, S. (2013) Concurrent Decadal Mesoscale Eddy Modulations in the Western North Pacific Subtropical Gyre. *J. Phys. Oceanogr*. 43, 344–358. doi: doi.org/10.1175/JPO-D-12-0133.1

Qiu, B., and Chen, S. (2014) Wind- versus Eddy-Forced Regional Sea Level Trends and Variability in the North Pacific Ocean. *J. Climate* 28, 1561–1577. doi: 10.1175/JCLI-D-14-00479.1

Soeyanto, E., Guo, X., Ono, J., and Miyazawa, Y. (2014) Interannual variations of Kuroshio transport in the East China Sea and its relation to the Pacific Decadal Oscillation and mesoscale eddies. *J. Geophys. Res. Oceans.* 119, 3595–3616. doi: 10.1002/2013JC009529

Wang, H., Liu, Q., Yan, H., Song, B., and Zhang, W. (2019) The interactions between surface Kuroshio transport and the eddy field east of Taiwan using satellite altimeter data. *Hai Yang Xue Bao* 38, 116–126. doi: 10.1007/s13131-019-1417-3

Wu, C. R., Wang, Y. L., Lin, Y. F., Chiang, T. L., and Wu, C.-C. (2016) Weakening of the Kuroshio Intrusion Into the South China Sea Under the Global Warming Hiatus. *IEEE J. Sel. Top. Appl. Earth Obs. Remote Sens.* 9, 5064–5070. doi: 10.1109/JSTARS.2016.2574941

Wu, C. R., Wang, Y. L., and Chao, S. Y., (2019) Disassociation of the Kuroshio Current with the Pacific Decadal Oscillation Since 1999. *Remote Sens.* 11, *2072–4292.*

Yan, X. M., and Sun, C. (2015) An altimetric transport index for Kuroshio inflow northeast of Taiwan Island. *Sci China Earth Sci.* 58, 697–706. doi: 10.1007/s11430-014-5024-z

Yan, X., Zhu, X. H., Pang, C., and Zhang, L. (2016) Effects of mesoscale eddies on the volume transport and branch pattern of the Kuroshio east of Taiwan. *J. Geophys. Res. Oceans* 121, 7683–7700. doi: 10.1002/2016JC012038

Yang, Y., Liu, C. T., Hu, J. H., and Koga, M. (1999) Taiwan Current (Kuroshio) and Impinging Eddies. *J. Oceanogr.* 55, 609–617.

Yang, Y. J., Jan, S., Chang, M. H., Wang, J., Mensah, V., Kuo, T. H., Tsai, C. J., Lee, C. Y., Andres, M., Centurioni, L. R., Tseng, Y. H., Liang, W. D., and Lai, J. W. (2015) Mean Structure and Fluctuations of the Kuroshio East of Taiwan from In Situ and Remote Observations. *Oceanography* 74–83. doi: 10.5670/oceanog.2015.83

Yang, D., Yin, B., Chai, F., Feng, X., Xue, H., Gao, G., and Yu, F. (2018) The onshore intrusion of Kuroshio subsurface water from February to July and a mechanism for the intrusion variation. *Prog. Oceanogr.* 167, 97–115. doi: 10.1016/j.pocean.2018.08.004

Zhang, D., Johns, W. E., Lee, T. N., Liu, C. T., and Antopp, R. (2001) The Kuroshio East of Taiwan: Modes of Variability and Relationship to Interior Ocean Mesoscale Eddies. *J. Phys. Oceanogr.* 31, 1054–1074. doi: 10.1175/1520-0485(2001)031<1054:TKEOTM>2.0.CO;2